CrystEngComm

PAPER

View Article Online
View Journal

Cite this: DOI: 10.1039/d5ce00437c

Improving the anti-hygroscopicity and safety of hydroxylamine pentazolate salt ($NH_3OH^+N_5^-$) by cocrystallization†

Lei Chen, ‡[a] Zhili Shen,‡[b] Deren Kong,[a] Chong Zhang, [b] Bingcheng Hu *[b] and Chao Gao *[b]

Received 23rd April 2025,
Accepted 3rd July 2025

DOI: 10.1039/d5ce00437c

rsc.li/crystengcomm

As a research hotspot in energetic materials, pentazolate salts have been restricted in widespread application due to their strong hygroscopicity and high sensitivity. In this study, a cocrystal of $NH_3OH^+N_5^-$ and 18-crown-6 (18C6) was prepared (1 : 1 molar ratio) *via* the solvent-evaporation method. It was characterized by single crystal X-ray diffraction, powder X-ray diffraction (PXRD), differential scanning calorimetry (DSC), and noncovalent interaction analysis. Crystal structure analysis shows that hydrogen bonds between NH_3OH^+ cations and the 18C6 ring drive cocrystal formation. Non-covalent interaction analysis shows that in $NH_3OH^+N_5^-$ and the cocrystal, N–H···N (63.9%) and N–H···O (43.0%) hydrogen bonds account for a significant proportion of the weak interactions, respectively. The results confirm that cocrystal formation improves the anti-hygroscopicity and safety of the compound (IS = 25 J, FS = 192 N).

Introduction

Energetic materials are vital energy sources for explosives, propellants, and pyrotechnics, underpinning strategic and tactical weapon systems.[1–3] However, traditional CHON-based energetic materials have theoretical detonation energies below twice the TNT equivalent, failing to meet future military demands. In contrast, all-nitrogen energetic materials,[4,5] leverage nitrogen bond energy disparities between N–N single bonds (159 kJ mol^{-1}), N=N double bonds (419 kJ mol^{-1}), and N≡N triple bonds (946 kJ mol^{-1}). Upon detonation, they release vast energy by forming stable N_2 gas, achieving theoretical outputs 6 to 8 times that of TNT, far surpassing CHON-based limits.[6–8] Their high formation enthalpy and clean byproducts further establish them as next-generation ultra-high-energy candidates.

Currently, all ambient-condition synthetic nitrogen compounds are ionic, including anions (N_3^-, N_5^-) and cations (N_5^+). Among these, the N_5^- anion offers a superior balance of higher energy than N_3^- and greater stability than N_5^+.[9,10] Its ring structure also facilitates assembly with counterions into energetic ionic salts with outstanding detonation properties.[11–15] For example, hydroxylamine pentazolate ($NH_3OH^+N_5^-$) achieves a theoretical detonation velocity of 9.93 km s^{-1} and an impact sensitivity of 6 J.[16] However, its severe hygroscopicity critically hinders development and practical use. While research suggests modifying the composition and crystal structure can reduce hygroscopicity,[17–19] finding effective solutions for $NH_3OH^+N_5^-$ remains a significant challenge in energetic materials research.

Cocrystals consist of two or more neutral molecules combined in a specific stoichiometric ratio.[20] Their molecular stacking is governed by noncovalent interactions like hydrogen bonding, π–π stacking, and van der Waals forces. Recently, cocrystallization has become a key method for synthesizing novel energetic compounds.[21–23] By forming new cocrystal structures, researchers can significantly influence key properties of energetic materials, including melting point, density, sensitivity, and other physicochemical characteristics.

We report a cocrystallization method synthesizing $NH_3OH^+N_5^-$ with 18-crown-6 ether (18C6). The $NH_3OH^+N_5^-$/18C6 cocrystal structure was determined by single-crystal X-ray diffraction, while its thermal decomposition, hygroscopicity, and mechanical sensitivity were comprehensively studied. Furthermore, we elucidate the contrasting intermolecular interactions that stabilize the cocrystal *versus* its raw components.

[a] *School of Mechanical Engineering, Nanjing University of Science and Technology, Nanjing, Jiangsu 210094, China*
[b] *School of Chemistry and Chemical Engineering, Nanjing University of Science and Technology, Nanjing, Jiangsu 210094, China. E-mail: hubc@njust.edu.cn, gaochao@njust.edu.cn*

† Electronic supplementary information (ESI) available. CCDC 2445937 and 2445981. For crystallographic data in CIF or other electronic format see DOI: https://doi.org/10.1039/d5ce00437c

‡ These authors contributed equally to this work.

Results and discussion

Single-crystal X-ray diffraction

The crystal structures of compounds $NH_3OH^+N_5^-$ and $NH_3OH^+N_5^-$/18C6 cocrystal are given in Fig. 1. The crystal structure of $NH_3OH^+N_5^-$ belongs to the monoclinic crystal system and in the $P12_1/c1$ space group. NH_3OH^+ cations and adjacent N_5^- anions are stabilized by two types of hydrogen bonds, O1–H···N and N6–H···N, with bond lengths ranging from 1.86 to 2.58 Å (Fig. 1a and b). As shown in Fig. 1c, the face-to-face stacking results from intra- and intermolecular hydrogen bonding and π–π interactions. The $NH_3OH^+N_5^-$/18C6 cocrystal crystallizes in the orthorhombic system, space group $P2_12_12_1$ (Z = 4). Its asymmetric unit comprises four NH_3OH^+ cations, six N_5^- anions, and four 18C6 molecules. The $NH_3OH^+N_5^-$/18C6 cocrystal features an NH_3OH^+ cation that is an excellent hydrogen bond donor, readily forming hydrogen bonds with the 18C6 ring oxygen atoms. As shown in Fig. 1d, six hydrogen bonds (N6–H···O) are formed between the NH_3OH^+ cation and the 18C6 ring, with bond lengths ranging from 1.87 to 2.54 Å. Additionally, the bond lengths of O7–H···N1 and O7–H···N2 between the NH_3OH^+ cations and N_5^- anions are 1.82 and 2.60 Å, respectively. Due to strong intramolecular hydrogen bonding, the average N–N bond length of N_5^- anions in the $NH_3OH^+N_5^-$/18C6 cocrystal is 1.30 Å, which is shorter than the average N–N bond length of 1.32 Å in $NH_3OH^+N_5^-$. The N atoms of the anions in $NH_3OH^+N_5^-$ are nearly coplanar, whereas those in the $NH_3OH^+N_5^-$/18C6 cocrystal exhibit a more twisted arrangement, as evidenced by the torsion angle of the five-membered ring (N2–N3–N4–N5 = −1.1° and N1–N2–N3–N4 = 1.0°). There is a dihedral angle of 39.99° between the N_5^- anions arranged in space, and the molecular stacking of the $NH_3OH^+N_5^-$/18C6 cocrystal exhibits a wave-like pattern (Fig. 1e and f). This indicates that intramolecular hydrogen bonding is the primary driving force for cocrystal formation. The crystals were irradiated using Mo Kα radiation (λ = 0.71073 nm) or using Cu Kα radiation (λ = 1.54178 nm). The structure was solved by direct methods with SHELXT program and refined by least-square methods with SHELXL-2014 program contained in OLEX2 suite. Selected crystal data are provided in the Table 1. The crystals were irradiated using Mo Kα radiation (λ = 0.71073 nm) or Cu Kα radiation (λ = 1.54178 nm). The structure was solved by direct methods using the SHELXT program and refined by least-squares methods using the SHELXL-2014 program within the OLEX2 suite.[24–26] Selected crystal data are presented in Table 1.

PXRD and IR spectroscopic analysis

The PXRD analysis of the raw materials and $NH_3OH^+N_5^-$/18C6 cocrystal are shown in Fig. 2a. The diffraction peaks of the $NH_3OH^+N_5^-$ were observed at 16.8°, 36.6°, and 38.4°, while those of the 18C6 pattern occurred at 15.6° and 17.5°. However, these strong characteristic diffraction peaks of the raw materials were absent in the $NH_3OH^+N_5^-$/18C6 cocrystal. Meanwhile, new diffraction peaks emerged at 6.25°, 13.3°, and 18.9° in the pattern of the $NH_3OH^+N_5^-$/18C6 cocrystal, suggesting that the cocrystal had transformed into a new substance structure from the two reactants in a certain proportion. In the IR spectrum of the $NH_3OH^+N_5^-$ (Fig. 2b), some peaks are observed at 3326, 1218 and 728 cm^{-1}. The IR spectrum of 18C6, displays absorption peaks

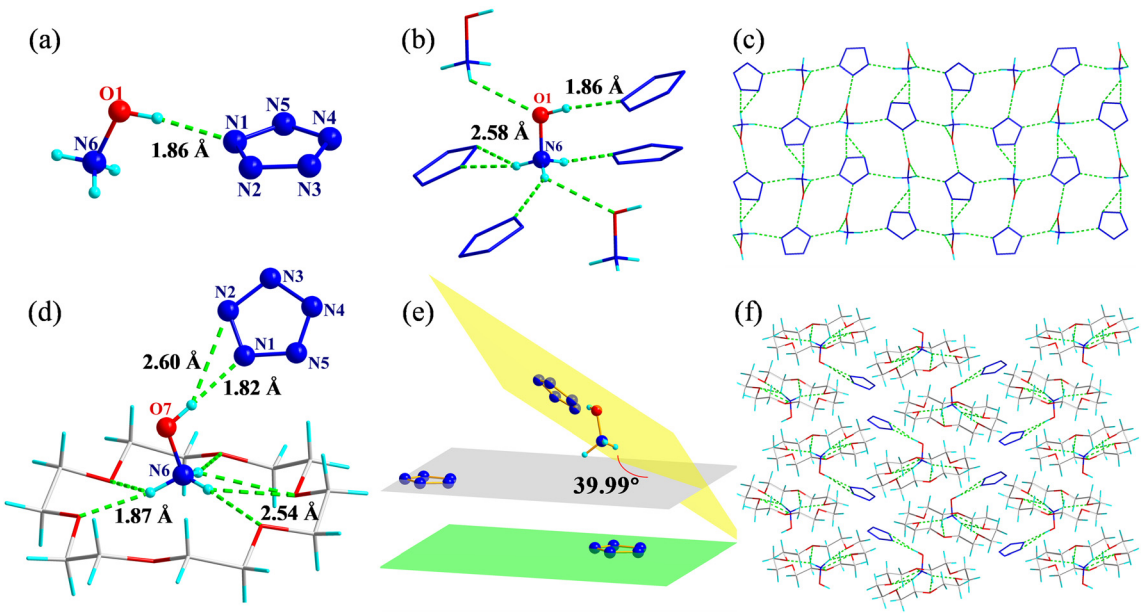

Fig. 1 (a) Crystal structure of $NH_3OH^+N_5^-$, (b) hydrogen bond network of cations in $NH_3OH^+N_5^-$, (c) stacking diagram of $NH_3OH^+N_5^-$, (d) crystal structure of $NH_3OH^+N_5^-$/18C6 cocrystal, (e) dihedral angle of $NH_3OH^+N_5^-$/18C6 cocrystal, (f) stacking diagram of $NH_3OH^+N_5^-$/18C6 cocrystal. Green lines in the crystal structure diagram represent hydrogen bonds.

Table 1 Crystallographic data for $NH_3OH^+N_5^-$ and $NH_3OH^+N_5^-$/18C6

Compound	$NH_3OH^+N_5^-$	$NH_3OH^+N_5^-$/18C6
Empirical formula	H_4N_6O	$C_{12}H_{28}N_6O_7$
Formula weight	104.09	368.40
Temperature (K)	193	193
Wavelength (Å)	0.71073	1.54178
Crystal system	Monoclinic	Orthorhombic
a (Å)	3.7631(2)	8.7794(3)
b (Å)	14.7655(7)	10.2396(4)
c (Å)	7.6847(4)	20.7518(8)
α (°)	90	90
β (°)	96.582(2)	90
γ (°)	90	90
Volume (Å^3)	424.18(4)	1865.54(12)
Crystal size (mm^3)	0.08 × 0.04 × 0.02	0.11 × 0.13 × 0.18

characteristic absorption peaks indicative of C–C and C–O stretching are present at 1495, 1355 and 859 cm^{-1}. However, in the $NH_3OH^+N_5^-$/18C6 cocrystal, different chemical components and the weak interactions result in shifts in the absorption peaks of raw materials. For instance, peaks shift from 1355 to 1350 cm^{-1}, 1218 to 1219 cm^{-1}, and 859 to 834 cm^{-1}. Notably, the peaks at 1218 and 1219 cm^{-1} correspond to the cyclic N_5^- anion absorption in the compound, aligning with previous findings.[27,28]

Thermal analysis

Thermal stability is one of the main factors to evaluate the safety of energetic materials. The thermal decomposition behavior of the $NH_3OH^+N_5^-$/18C6 cocrystal from 30 to 500 °C was investigated using differential scanning calorimetry (DSC). Approximately 0.3 mg of sample was placed in an 85 μL alumina crucible, the and test was performed under an argon atmosphere with a flow rate of 50 mL min $^{-1}$ and heating rates of 2, 5, 10 K min $^{-1}$ and 15 K min $^{-1}$ (Fig. 3a). The DSC curve shows that the exothermic peak temperature increases with the heating rate. Under a temperature rise test condition of 5 K min $^{-1}$, the thermal analysis of dried anhydrous compounds ($NH_3OH^+N_5^-$ and its cocrystal) is shown in Fig. 3b. The thermal stability (T_d = 146.2 °C) of the $NH_3OH^+N_5^-$/18C6 cocrystal is higher than that of the raw material $NH_3OH^+N_5^-$ (T_d = 119.3 °C), yet it takes longer for cocrystal to reach the exothermic peak, which suggests that its energy release is slower. This result indicates that the composition and weak interactions in the cocrystal structure influence the thermal decomposition behavior of compounds. As listed in Table 2, the activation energy of $NH_3OH^+N_5^-$/18C6 cocrystal, calculated using the Kissinger and Ozawa formulas (Fig. 3c and d), was 55.68 kJ mol^{-1} and 62.65 kJ mol^{-1}, respectively.

Noncovalent interaction analysis

Understanding the sensitivity of energetic materials to mechanical impact and friction plays a crucial role in evaluating their safety throughout storage, transportation, and use.[29] The mechanical sensitivities of the raw materials and the $NH_3OH^+N_5^-$/18C6 cocrystal were tested using the standard BAM method. The impact sensitivity of $NH_3OH^+N_5^-$ is 6 J, while its friction sensitivity is 60 N. By comparison, the $NH_3OH^+N_5^-$/18C6 cocrystal demonstrates an impact sensitivity of 25 J and a friction sensitivity of 192 N. These results indicate that cocrystal formation significantly affects the mechanical sensitivity. To explore the reasons behind the sensitivity changes, two-dimensional (2D) fingerprint analysis and Hirshfeld surface analysis were conducted to examine the intramolecular interaction differences between the raw materials and the cocrystal structure (Fig. 4). Generally, red and blue regions on Hirshfeld surfaces represent strong and weak interatomic contacts, respectively.[30,31] As shown in Fig. 4a, the Hirshfeld surface of the $NH_3OH^+N_5^-$ exhibits a polygonal shape. In contrast, the Hirshfeld surface of the $NH_3OH^+N_5^-$/18C6 cocrystal is more irregular, with a distinct red region appearing between the NH_3OH^+ cations and the 18C6 ring (Fig. 4c).

Fig. 4b and d illustrate the types of intermolecular interactions in the $NH_3OH^+N_5^-$ and $NH_3OH^+N_5^-$/18C6 cocrystal *via* 2D fingerprint plots, while the ratios of interactions such as H···O, H···H, and O···H are shown in Fig. 4b and d. In the $NH_3OH^+N_5^-$, the H···N interaction accounts for 63.9%, while the H···O interaction accounts for 10.7%, corresponding to the sharp spikes in the lower-left region of the 2D fingerprint plots. In the $NH_3OH^+N_5^-$/18C6 cocrystal, the H···O and H···H interactions are

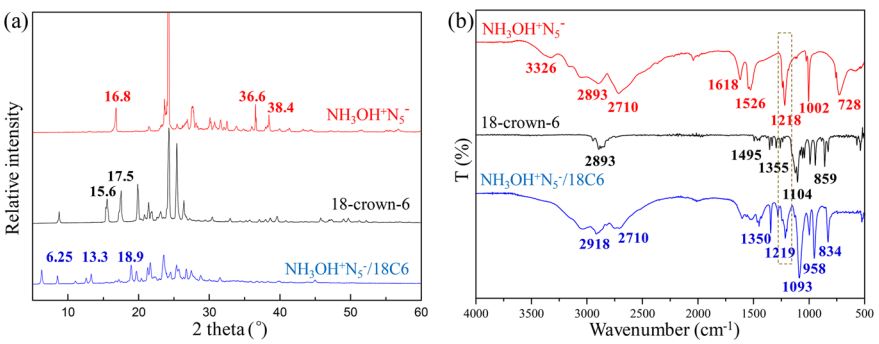

Fig. 2 The PXRD pattern (a) and IR spectra (b) of the raw materials and $NH_3OH^+N_5^-$/18C6 cocrystal, respectively.

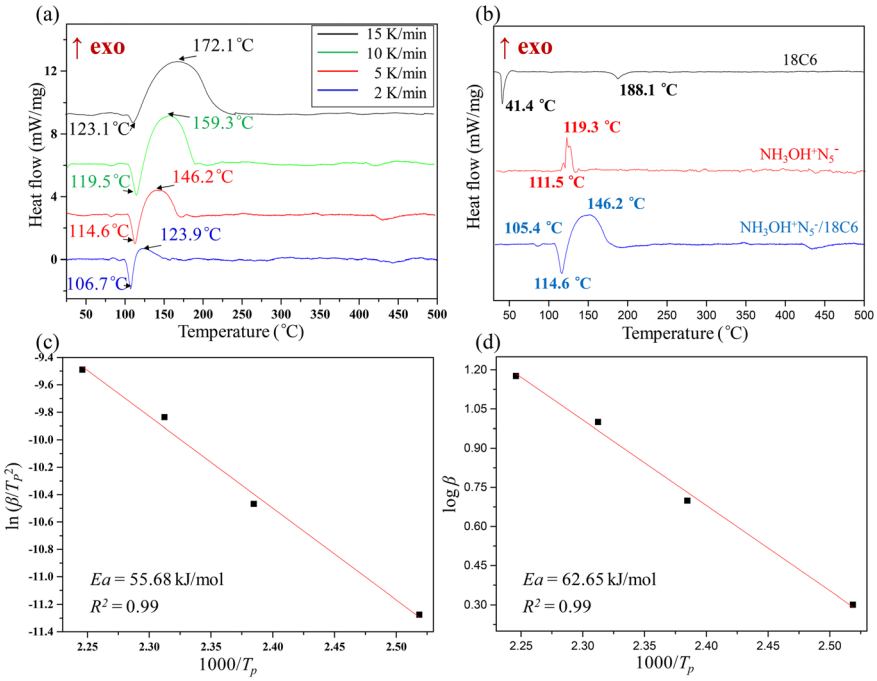

Fig. 3 (a) The DSC curves of the $NH_3OH^+N_5^-$/18C6 cocrystal at heating rates of 2, 5, 10 K min^{-1} and 15 K min^{-1}. (b) The DSC curves of the raw materials and the $NH_3OH^+N_5^-$/18C6 cocrystal at a scan rate of 5 K min^{-1}. Activation energy of $NH_3OH^+N_5^-$/18C6 cocrystal calculated by the Kissinger method (c) and the Ozawa method (d).

43.0% and 23.8%, respectively. These data suggest strong intermolecular interactions between NH_3OH^+ cations and the 18C6 rings within the molecular stacking structure. Additionally, the region corresponding to hydrogen bonds in the 2D fingerprint appears brighter, suggesting that hydrogen bonding interactions play a significant role in the structural stability of both compounds.

To further uncover the intermolecular and intramolecular interactions and comprehensively investigate their effects on crystal packing, noncovalent interaction (NCI) plots for $NH_3OH^+N_5^-$ and the $NH_3OH^+N_5^-$/18C6 cocrystal were analyzed based on the electron density of their real spatial structure.[32,33] In Fig. 5a and b, green and light brown isosurfaces appear between ions, indicating weak interactions in the molecular stacking of $NH_3OH^+N_5^-$ and the $NH_3OH^+N_5^-$/18C6 cocrystal, such as π–π interactions. The presence of π–π interactions causes the anion arrangement in the $NH_3OH^+N_5^-$ to be almost parallel, while the anion arrangement in the cocrystal has a large dihedral angle. Additionally, hydrogen bonding interactions are observed between the H atom of the NH_3OH^+ cation, the N atom of the N_5^- anion, and the O atom of the 18C6 ring, corresponding to the blue patches in the NCI plots. Therefore, the differences between hydrogen bonds and van der Waals interactions affect the stacking mode and stability of the two compounds.

Table 2 Kinetic and thermal stability parameters obtained using the Kissinger and Ozawa methods

β/K min^{-1}	T_p/K	Kissinger method		Ozawa method	
		E_K/kJ mol^{-1}	R	E_O/kJ mol^{-1}	R
2	397.05	55.68	0.99	62.65	0.99
5	419.35				
10	432.45				
15	445.25				

Hygroscopicity analysis

Scanning electron microscopy (SEM) anlysis revealed the morphologies of $NH_3OH^+N_5^-$ and the $NH_3OH^+N_5^-$/18C6 cocrystal. $NH_3OH^+N_5^-$ has a flaky shape with a cracked surface (Fig. 6a), whereas the cocrystal shows a layered structure with a tightly packed surface (Fig. 6b). Fig. 6c and d show the appearance state of two compounds before and after hygroscopic testing. $NH_3OH^+N_5^-$ turns from white granules to a solution in about 13 hours of exposure, while the surface of $NH_3OH^+N_5^-$/18C6 cocrystal remains mostly unchanged without obvious caking. The mass changes of the two samples were evaluated gravimetrically at 30 °C and 75% relative humidity, and the hygroscopicity curves are displayed in Fig. 6e. $NH_3OH^+N_5^-$ has a maximum hygroscopicity of 45.1%, while that of cocrystal is only 8.3%, with a much slower hygroscopic rate. These results show that cocrystal formation alters the molecular stacking and surface morphology. Also, the oxygen atoms of the crown ether molecule form N–H···O hydrogen bonds with the NH_3OH^+ ion, lowering the chance of NH_3OH^+ ions interacting with water molecules in the air. Thus, $NH_3OH^+N_5^-$/18C6

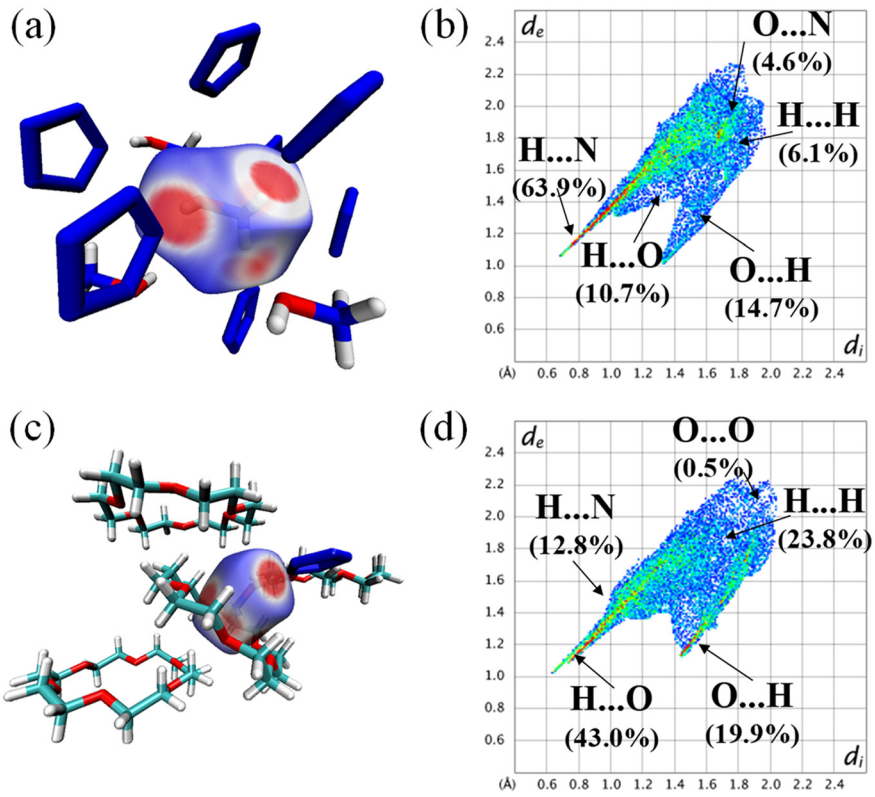

Fig. 4 The Hirshfeld surfaces of $NH_3OH^+N_5^-$ (a) and the $NH_3OH^+N_5^-$/18C6 cocrystal (c), 2D fingerprint plots and percentage contributions of molecular interactions of $NH_3OH^+N_5^-$ (b) and the $NH_3OH^+N_5^-$/18C6 cocrystal (d) in crystal stacking.

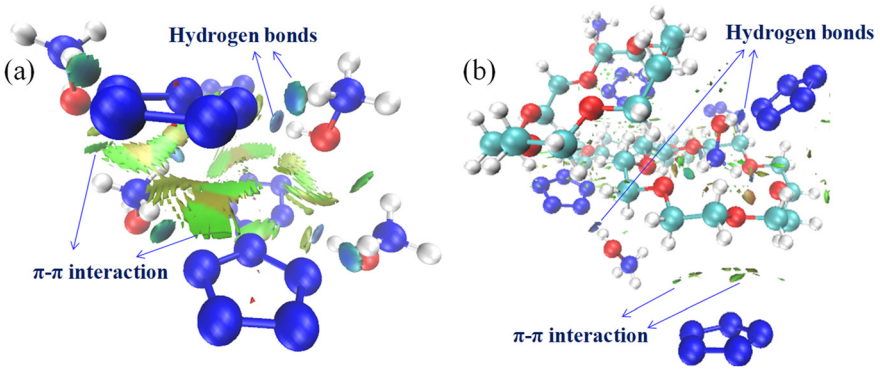

Fig. 5 NCI plots. Color-mapped reduced density gradient (RDG) isosurfaces for $NH_3OH^+N_5^-$ (a) and the $NH_3OH^+N_5^-$/18C6 cocrystal (b), respectively. Blue: strong attraction; green: van der Waals interaction; red: strong repulsion.

cocrystal decreases the water adsorption rate, thereby improving the anti-hygroscopicity of compound.

Experimental

Materials and instruments

All chemicals from commercial sources were analytical grade and used as received without further purification. $NH_3OH^+N_5^-$ was prepared according to the previously reported procedure.[16]

Thermal property measurements were obtained on DSC (NETZSCH STA 449F5) at a scan rate of 2, 5, 10 K min^{-1} and 15 K min^{-1} in closed Al containers with an argon flow of 50 mL min^{-1}. FT-IR spectra were recorded on a Thermo Nicolet IS10 instrument. The crystal data of $NH_3OH^+N_5^-$ and $NH_3OH^+N_5^-$/18C6 were collected with a Bruker D8 VENTURE single-crystal diffractometer at 193 K. The powder X-ray diffraction (PXRD) patterns of the raw materials and the $NH_3OH^+N_5^-$/18C6 cocrystal were recorded using a Rigaku miniflex diffractometer, operating in the 2θ range of 5° to 60° with a step size of 0.01°.

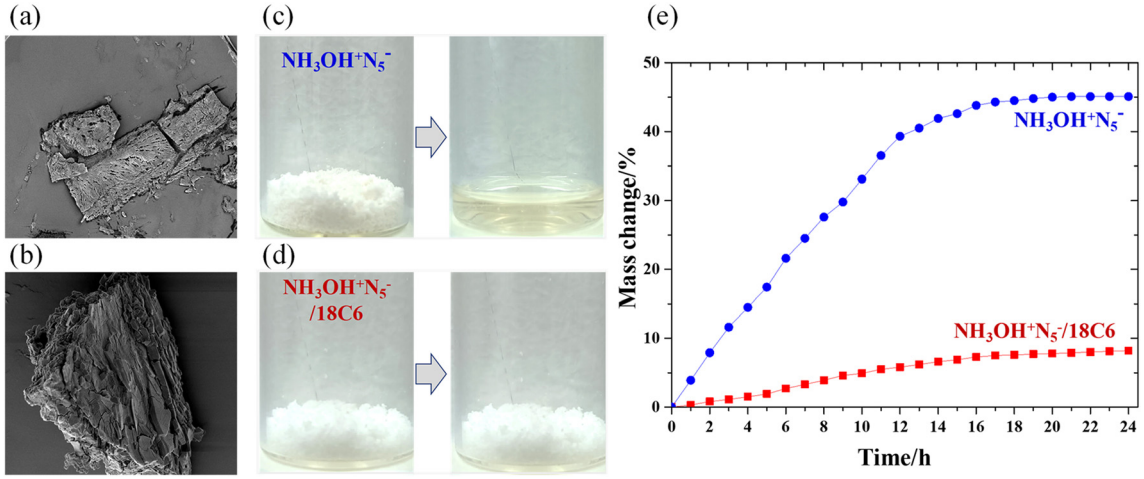

Fig. 6 (a and b) The morphology of $NH_3OH^+N_5^-$ and $NH_3OH^+N_5^-$/18C6 cocrystal, respectively, (c and d) Appearance state of $NH_3OH^+N_5^-$ and $NH_3OH^+N_5^-$/18C6 cocrystal, respectively, (e) Hygroscopicity rate curves for the $NH_3OH^+N_5^-$ and the $NH_3OH^+N_5^-$/18C6 cocrystal.

Preparation of the cocrystal

$NH_3OH^+N_5^-$ (2 mmol) and 18C6 (2 mmol) were dissolved in a mixture of deionized water (2 mL) and methanol (5 mL), and the solution was stirred at 30 °C for 1 h. Subsequently, the undissolved substance was removed *via* filtration, and the filtrate was then evaporated at room temperature to yield the $NH_3OH^+N_5^-$/18C6 cocrystal.

Conclusions

In summary, the $NH_3OH^+N_5^-$/18C6 cocrystal was prepared using the solvent-evaporation method and crystallizes in the orthorhombic system with the $P2_12_12_1$ space group. The main driving force for cocrystal formation is the N–H···O hydrogen bonds between NH_3OH^+ cations and crown ether molecules, which have bond lengths ranging from 1.87 to 2.54 Å. The analysis of Noncovalent interactions shows that in the $NH_3OH^+N_5^-$ molecular structure, the NH_3OH^+ cations primarily interact weakly with three neighboring NH_3OH^+ cations and eight N_5^- anions. In contrast, in the $NH_3OH^+N_5^-$/18C6 cocrystal structure, the NH_3OH^+ cations mainly have weak interactions with four crown ether molecules and one N_5^- anion. These distinct stacking modes and interaction strengths result in $NH_3OH^+N_5^-$ having an impact sensitivity of 6 J and a friction sensitivity of 60 N, while cocrystal has an impact sensitivity of 25 J and a friction sensitivity of 192 N. Additionally, the N–H···O hydrogen bonds in the cocrystal structure reduce the water adsorption rate of compound. This indicates that cocrystal formation is a promising strategy for improving the anti-hygroscopicity of pentazolate salts.

Data availability

Crystallographic data for the $NH_3OH^+N_5^-$/18C6 cocrystal and $NH_3OH^+N_5^-$ have been deposited at the CCDC under numbers 2445937 and 2445981.

Author contributions

L. C.: data curation, methodology, conceptualization, and writing-original draft. Z. S.: formal analysis, validation and conceptualization. D. K.: investigation and formal analysis. C. Z.: validation and formal analysis. C. G., B. H.: conceptualization, supervision, methodology, and writing-review & editing.

Conflicts of interest

There are no conflicts of interest to declare.

Acknowledgements

The authors gratefully acknowledge the financial support provided by the National Natural Science Foundation of China (No. 22205109, and 22375097) and the Fundamental Research Funds for the Central Universities (No. 30922010812).

Notes and references

1 Y. Qu and S. P. Babailov, *J. Mater. Chem. A*, 2018, **6**, 1915–1940.
2 J. Wang, R. Lv, H. Wang, Q. Zhang, S. Huang and K. Wang, *Chem. Eng. J.*, 2025, **503**, 158233.
3 Q. Lai, L. Pei, T. Fei, P. Yin, S. Pang and J. M. Shreeve, *Nat. Commun.*, 2022, **13**, 6937.
4 K. Zhong and C. Zhang, *Chem. Eng. J.*, 2024, **483**, 149202.
5 S. Liu, L. Zhao, M. Yao, M. Miao and B. Liu, *Adv. Sci.*, 2020, **7**, 1902320.
6 X. Wu, Q. Yu, Y. Li, J. Xu and J. Zhang, *Chem. Eng. J.*, 2023, **454**, 140359.
7 B. A. Steele, E. Stavrou, J. C. Crowhurst, J. M. Zaug, V. B. Prakapenka and I. I. Oleynik, *Chem. Mater.*, 2017, **29**, 735–741.
8 M. Arhangelskis, A. D. Katsenis, A. J. Morris and T. Friščić, *Chem. Sci.*, 2018, **9**, 3367–3375.

9 K. O. Christe, *Science*, 2017, **355**, 351.
10 D. R. Wozniak and D. G. Piercey, *Engineering*, 2020, **6**, 981–991.
11 W. Zhang, K. Wang, J. Li, Z. Lin, S. Song, S. Huang, Y. Liu, F. Nie and Q. Zhang, *Angew. Chem., Int. Ed.*, 2018, **57**, 2592–2595.
12 C. Sun, C. Zhang, C. Jiang, C. Yang, Y. Du, Y. Zhao, B. Hu, Z. Zheng and K. O. Christe, *Nat. Commun.*, 2018, **9**, 1269.
13 P. Wang, Y. Xu, Q. Lin and M. Lu, *Chem. Soc. Rev.*, 2018, **47**, 7522–7538.
14 C. Zhang, C. Sun, B. Hu, C. Yu and M. Lu, *Science*, 2017, **355**, 374–376.
15 W. Yi, L. Zhao, X. Liu, X. Chen, Y. Zheng and M. Miao, *Mater. Des.*, 2020, **193**, 108820.
16 C. Yang, C. Zhang, Z. Zheng, C. Jiang, J. Luo, Y. Du, B. Hu, C. Sun and K. O. Christe, *J. Am. Chem. Soc.*, 2018, **140**, 16488–16494.
17 H. Li, L. Li, J. Sun, J. Han, L. Yang, X. Ren and W. Tong, *Inorg. Chem.*, 2024, **63**, 16713–16725.
18 F. Chen, C. Xuan, Q. Lu, L. Xiao, J. Yang, Y. Hu, G. Zhang, Y. Wang, F. Zhao, G. Hao and W. Jiang, *Def. Technol.*, 2023, **19**, 163–195.
19 Z. Ren, X. Chen, G. Yu, Y. Wang, B. Chen and Z. Zhou, *CrystEngComm*, 2020, **22**, 5237–5244.
20 Y. Tan, Z. Yang, H. Wang, H. Li, F. Nie, Y. Liu and Y. Yu, *Cryst. Growth Des.*, 2019, **19**, 4476–4482.
21 V. B. Patil, P. Bělina, W. A. Trzcinski and S. Zemana, *Chem. Eng. J.*, 2024, **483**, 149029.
22 F. Meng, Z. Ye, H. Zhu, L. Sun, M. Lu and Y. Xu, *Dalton Trans.*, 2025, **54**, 1307–1319.
23 C. Yang, L. Chen, W. Wu, C. Zhang, C. Sun, Y. Du and B. Hu, *ACS Appl. Energy Mater.*, 2021, **4**, 146–153.
24 G. Sheldrick, *Acta Crystallogr., Sect. A: Found. Adv.*, 2015, **71**, 3–8.
25 S. Datta, P. Ghorai, M. Chattopadhyay, N. Jana, P. Banerjee and M. Mir, *Cryst. Growth Des.*, 2024, **24**, 8645–8654.
26 W. Song, R. Justice, C. Jones, V. Grassian and S. Larsen, *Langmuir*, 2004, **20**, 4696–4702.
27 C. Zhang, C. Yang, B. Hu, C. Yu, Z. Zheng and C. Sun, *Angew. Chem., Int. Ed.*, 2017, **56**, 4512–4514.
28 Y. Xu, Q. Lin, P. Wang and M. Lu, *Chem. – Asian J.*, 2018, **13**, 1669–1673.
29 C. Yang, L. Chen, S. Chen, W. Wu, W. Yuan, J. Yao, C. Zhang, C. Sun, Y. Du and B. Hu, *Cryst. Growth Des.*, 2021, **21**, 4329–4336.
30 M. A. Spackman and D. Jayatilaka, *CrystEngComm*, 2009, **11**, 19–32.
31 T. Lu and F. Chen, *J. Comput. Chem.*, 2012, **33**, 580–592.
32 R. Bu, Y. Xiong and C. Zhang, *Cryst. Growth Des.*, 2020, **20**, 2824–2841.
33 F. Jiao, Y. Xiong, H. Li and C. Zhang, *CrystEngComm*, 2018, **20**, 1757–1768.